Progress In Electromagnetics Research Letters, Vol. 110, 37–45, 2023

Polarization Insensitive Dual Band FSS for S-Band and X-Band Applications

Anandan Suganya and Rajesh Natarajan*

Abstract—This paper presents the design of dual-band spatial filter for shielding S band and X band wireless signals. The proposed Frequency Selective Surface (FSS) geometry consisting of a square loop convoluted with four strips positioned along the conducting loop. The FSS is aimed to reject WLAN/S-band (2.64 GHz) and X-band (8.3 GHz) wireless signals. The proposed FSS is tested for its angular stability by considering the wave incidence at various angles between 0° and 60°. It is also tested for its polarization insensitive feature via TE mode and TM mode. The prototype FSS is printed on an FR-4 substrate with 1.6 mm thickness and the unit cell footprint of 14.8 mm and tested in an anechoic chamber. The working principle is explained through surface current distribution and the equivalent circuit model of the FSS. Measured results have better similarity with the simulated results.

1. INTRODUCTION

Frequency Selective Surface (FSS) is one of the favourite research topics among the researchers due to its wide application in electromagnetics (EM) especially in shielding applications. The spatial filters can have either a passband or stopband characteristics based on the implementation of inductive or capacitive patches. FSSs serve as filters, radomes as protective cover for the antenna, shielding enclosure, absorbers, and recently there have been intelligent surfaces. FSS implementations are available with single layer metallic patches for miniaturized unit cell design, dual band shielding with convoluted patches. Similarly, the bandwidth of an FSS can be improved with double layer implementations with similar elements and also dissimilar elements. FSS perturbed via holes gives 2.5D dimensional implementation which gives ultimate miniaturization of the unit cell.

To achieve dual-band passband responses at low frequencies, a dual-concentric square element with two different slot sizes is built [1]. Compactness is achieved via anchor shaped loop elements [2] for Global System for Mobile Communication (GSM)/Wireless Local Area Network (WLAN) indoor shield with miniaturization about $\lambda/13$ of unit cell dimension. Crooked cross geometry deployed with convolved branch elements in [3] gives high level shielding to the closely separated two frequencies with sufficient bandwidth. Sensitivity of the FSS is tested till 60° in both TE and TM modes. A dual polarized dual band FSS is proposed with crossed dipoles convolved with annular ring at the dipole edges in [4]. Symmetric nature of the unit cell takes care of angular and polarization independency. A novel double square loop unit cell is knitted on both sides to enhance the inductance and capacitance, and the layers are connected by vias in [5] to have excellent miniaturization in 2.5D implementation. Shielding effectiveness of the shield is displayed up to 60° of angular incidence. Two dissimilar conducting patches in [6] exhibit dual stopband characteristics at C band and WLAN band. An annular ring is used on both sides of the substrate to implement a three-dimensional FSS. This gives additional freedom and control over the bandwidth of the FSS in [7]. A tri-band FSS reported in [8] used Jerusalem cross, rotated Jerusalem cross, and un-rotated Jerusalem element printed on subsequent layers on the

Received 5 December 2022, Accepted 18 March 2023, Scheduled 7 April 2023
* Corresponding author: Rajesh Natarajan (rajeshnatarajan44@gmail.com).
The authors are with the School of Electronics Engineering, Vellore Institute of Technology, Vellore, TamilNadu 632014, India.

substrate. Very small dimension of the FSS only about $0.078\lambda_0$ is at the lower operating frequency among 0.9/1.8/2.4 GHz. Better miniaturization with meander line unit cells provides dual band shielding with frequency ratio 1.29 in [9]. A low-profile dual-band frequency selective surface (FSS) for GSM application shielding employs modified double square loop elements on a paper substrate, providing band stop response at 930 and 1720 MHz with 18 dB shielding efficiency for a bandwidth of 100 and 173 MHz. It also has an angular stability up to 60 degrees for both polarizations [10].

The covered literature concentrates on compactness by increasing the electrical length, two layer or 2D dimensional structure for bandwidth improvement and additional compactness. The remaining half of literature concentrates on the FSS implementation for different applications in electromagnetics. Convoluted square elements on a single side substrate provide better attenuation of X band signals in [11]. Equivalent circuit model validated the stable operation up to 60° of incidence. Triple stopband characteristic obtained via a two-layer square loop structure and a modified square loop structure on either side of the substrate in [12]. Square loops and metallic grids imposed on a layered substrate give dual stopband characteristics at X and Ka bands with large frequency separation in [13]. The unit cell designed with a square arm and extended stubs exhibits two closely spaced resonances in [14] with a small footprint of 0.021λ compared with lower operating frequency. Apart from these applications, FSS is also implemented for reflective and transmissive array via hexagonal and Y shaped stubs in satellite applications [15]. This dual polarized implementation proves the stability up to 80° of incident angle. A rectangular split ring resonator embedded with a T stub formed the metamaterials in [16]. FSS is a miniaturized structure made up of hexagonal metallic lines, and hexagonal patches provide stable performance and angular stability [17]. A miniaturized FSS with convoluted interlaced and extending four dipoles into the adjacent element were able to produce the same response at 1.19 GHz resonance frequency [18]. FSSs are implemented for flexible applications [19] as well as wideband application [20].

The paper is organized with the unit cell design in Section 2 with design evolution. An anechoic chamber setup for measurement with the result and discussion is shown in Section 3. Conclusion and future work are presented in the last section. Simulations are carried out through CST microwave studio. Single unit cell designed on CST and frequency domain solver is used to verify the transmission behaviour of the FSS. Floquet modes are fixed on either side of the substrate with 5-unit distance, and periodic boundary is used on horizontal planes (x and y).

2. FSS UNIT CELL DESIGN

2.1. Unit Cell Design

Square loop and crossed dipoles are prominent in FSS design because of its angular stability and polarization stability behaviour. To further explore its implementation as dual band nature, many fusion structures were made with square loop. Some of the standard unit cells are cross, Jerusalem cross, swastika shaped unit cells. The unit cell selection was made based on the parametric study, shown in Fig. 1. It shows the transmission coefficient responses of the standard unit cells. The application band is aimed at S band and X band in this paper. Hence, the loop and spitted strips are convoluted together to obtain the stopband behaviour of the FSS.

Split strips are the modified versions of the crossed dipoles by incorporating a discontinuity at the centre so that it can work at the X band. Fig. 2 shows the geometry of the proposed FSS unit cell. The dimension of the unit cell is 14.8 mm × 14.8 mm along the length and width to accommodate two largely spaced elements. The length of the split strip is chosen as $L1 = 6.5$ mm. The distance between the split end strips ($g1$) is 0.4 mm, and the inter element spacing between the unit cells is also 0.4 mm to avoid mutual coupling.

The unit cell behaviour is understood with the surface current diagram given in Fig. 3. The unit cell is exposed with a plane wave for different incident angles, and the current distribution is presented for $\theta = 0$ deg. The outer loop is holding the current for the S band, and the inner strips are holding the maximum current for the X band. The unit cell dimension at the operating frequency is only $0.098\lambda_0 \times 0.098\lambda_0$ where λ_0 is the lower operating frequency.

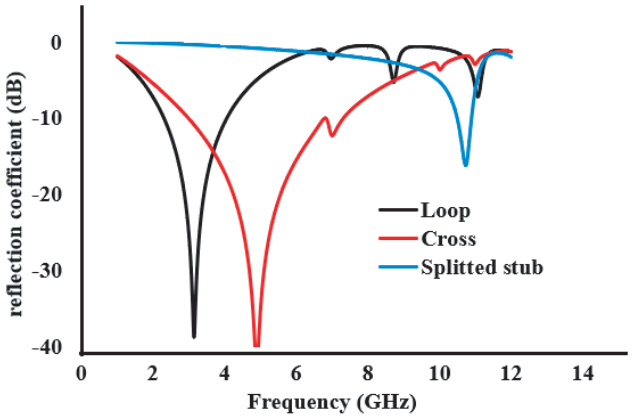

Figure 1. Parametric sweep with standard structures involved in the unit cell design.

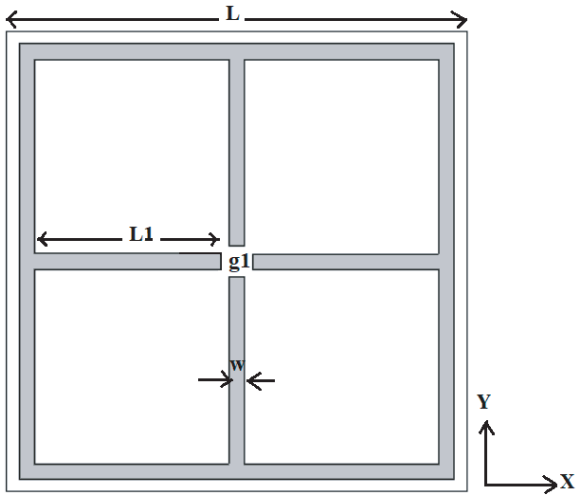

Figure 2. Unit cell dimensions of the proposed FSS.

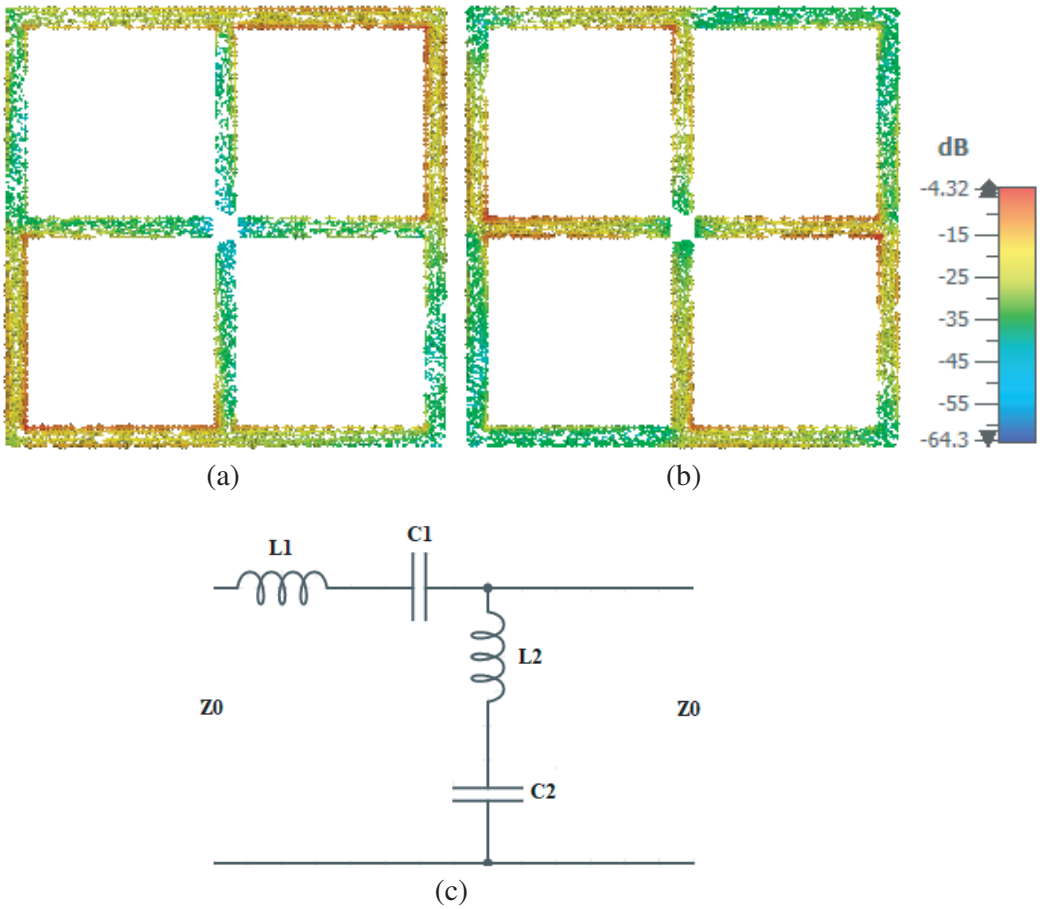

Figure 3. Surface current distributions of the unit cell in TE mode. (a) 2.6 GHz. (b) 8.3 GHz. (c) Equivalent circuit of the FSS.

2.2. FSS Unit Cell — Equivalent Circuit

The equivalent circuit of the proposed FSS unit cell is presented in Fig. 3(c). The first resonance is attributed to the outer square loop where L1 is proportional to the effective length of the square loop (L1), and the capacitance C1 is attributed to the gap of adjacent unit cells. This is derived to be $L1 = 0.2\,\text{nH}$ and $C1 = 17.9\,\text{pF}$ from CST. This provides the first stopband at 2.6 GHz. The dipoles at the corners contribute the inductance L2 and the inter element spacing contributes C2. The centre gap gives the capacitance connected with the outer loop which gives resonance at 8.3 GHz. The values of the lumped parameters are extracted from CST and are $L2 = 7.8\,\text{nH}$ and $C2 = 0.04\,\text{pF}$. This gives the second resonance of the unit cell. Since it is a single layer FSS, the thickness of the substrate is neglected in the equivalent circuit model which is depicted in Fig. 3(c).

2.3. Effectiveness of the FSS

Figure 4 depicts the reflection and transmission curves of the proposed FSS, which is used to assess its performance for TE (y-polarized) and TM (x-polarized) behaviour. It is observed that there is a passband operating between 3.97 and 5.73 GHz, with two stopbands on either side of it. The stopband on the left attenuates the frequency range from 2.60 to 3.95 GHz by −10 dB reference, and the stopband on the right does the same for the range from 8.2 to 12.4 GHz.

The performance of the two stopbands can be further quantified by plotting the shielding efficient as

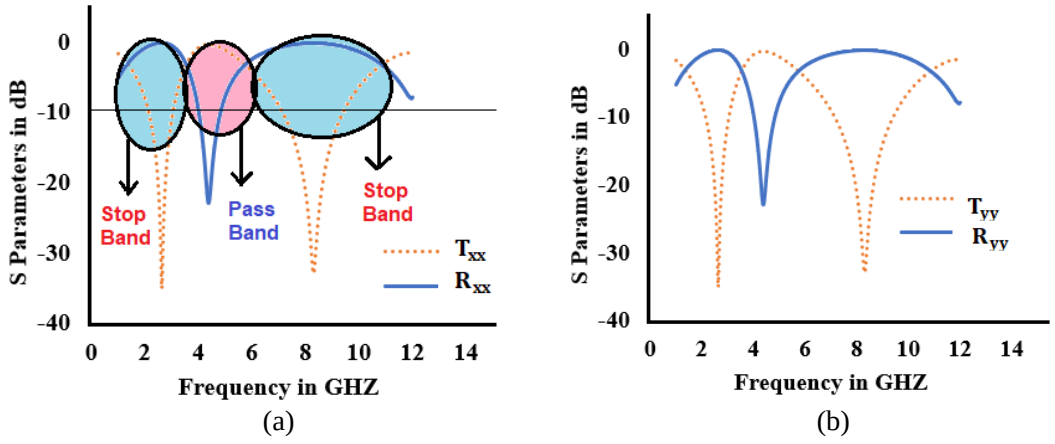

Figure 4. (a) Proposed FSS's reflection and transmission characteristics for x polarization. (b) Proposed FSS's reflection and transmission characteristics for y-polarization.

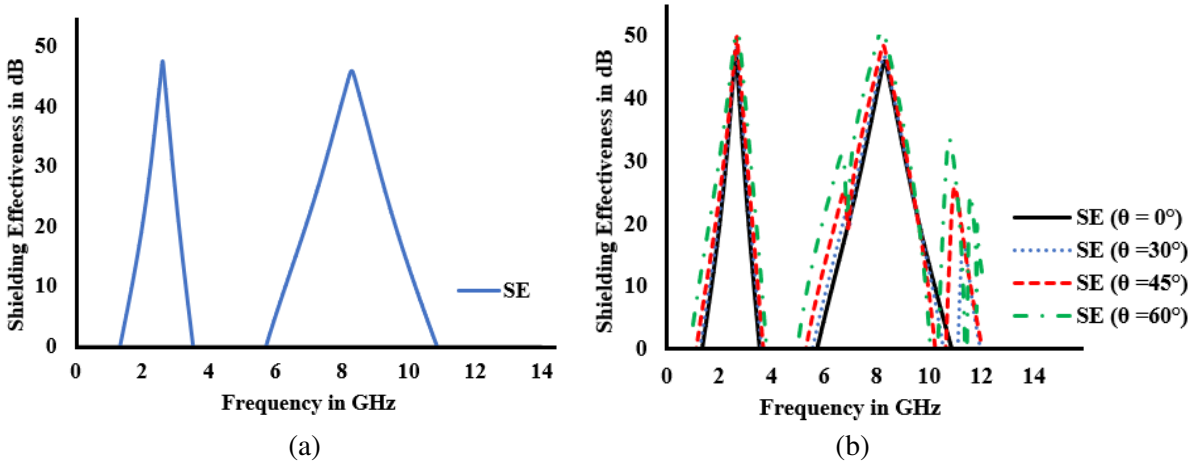

Figure 5. (a) Shielding Effectiveness of the FSS. (b) Polarization and angular stability of SE.

in [23], which is stated as the ratio between the incident and transmitted electric fields in Equation (1).

$$SE = 20\log\left|\frac{\text{Incident Electric Field}}{\text{Transmitted Electric Field}}\right| \tag{1}$$

The FSS provides a high level of shielding across the band of interest, with maximum values of 47.20 dB at 2.6 GHz and 45.7 dB at 8.3 GHz respectively which is shown in Fig. 5(a). It is preferable to have a response that is not polarization dependent in EM shielding applications. In other words, when being incident on the FSS, every polarization should experience the same filtered reaction. It is clear from Fig. 5(b) that the symmetry in the geometry of the planned structure renders it insensitive to the type of polarization illuminating the surface, demonstrating that the disclosed FSS is polarization insensitive.

3. RESULTS AND DISCUSSION

Transmission coefficient behaviour of the FSS is studied to verify the effectiveness of the shield. The unit cell is chosen as symmetric so that it provides uniform behaviour on TE and TM modes. The simulation is performed at various EM wave incidence angles to determine the FSS's angular stability; the results show that the proposed FSS provides stable angular stability for TE and TM propagation modes at various angles up to 60 degrees for incident and polarization angle. The polarization angle (Φ) and incidence angle (θ) of the plane wave of the FSS are mathematically expressed by Equations (2) and (3), respectively [21], and are depicted in Fig. 6. The simulated transmission coefficients for TE mode are shown in Figs. 7(a) and 7(b), and they are almost identical for the incident angle (θ) and polarization angle (Φ) from 0 deg to 60 deg. From Figs. 7(a) and 7(b), the dual mode FSS provides stopband at 2.64 GHz and 8.3 GHz, with bandwidths of 0.2 GHz and 0.9 GHz measured at -10 dB reference level. While the TE mode response is observed, it is stable throughout the bandwidth. When the unit cells are illuminated beyond 45 degrees, there exists vertical current which causes additional ripples. The transmission behaviour of the FSS is identical in TM mode also for the angle between 0° and 60°

$$\hat{\theta} = \cos\theta\cos\Phi\hat{x} + \cos\theta\sin\Phi\hat{y} - \sin\theta\hat{z} \tag{2}$$

$$\hat{\Phi} = \sin\Phi\hat{x} + \cos\Phi\hat{y} \tag{3}$$

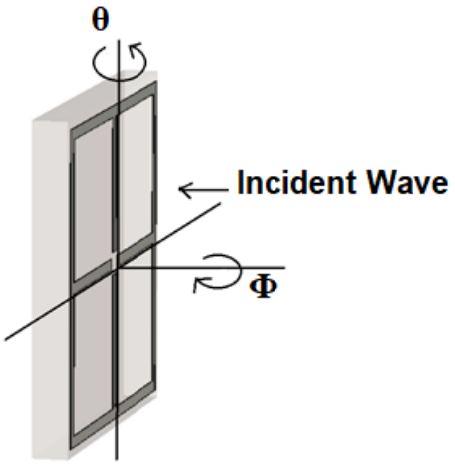

Figure 6. Polarization and incidence angle illustration of the proposed design.

Maximum predicted relative deviation is described by the following formula [22].

$$\Delta f = \left|\frac{f_z - f_{oblique}}{f_z}\right| \tag{4}$$

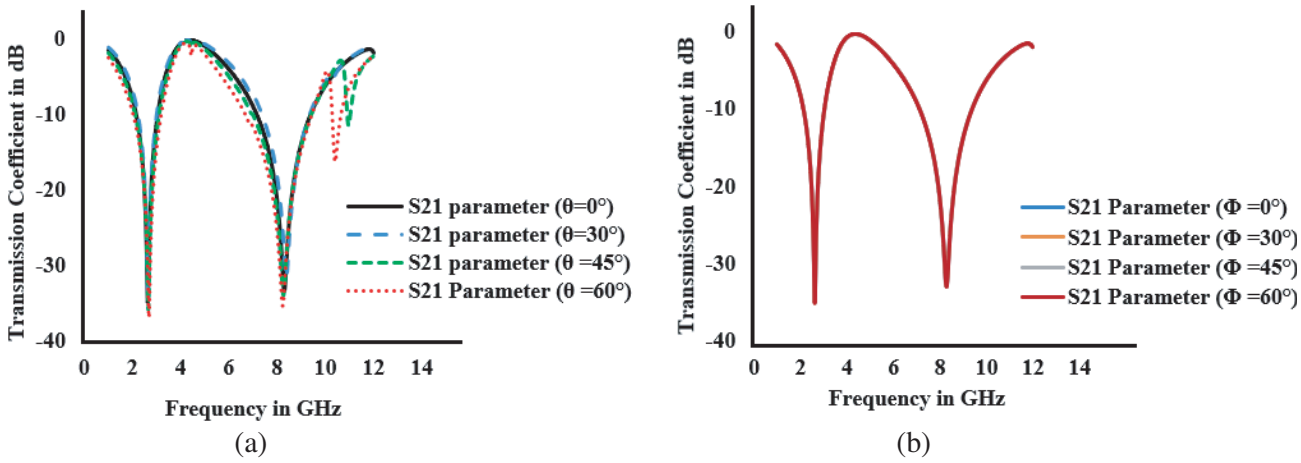

Figure 7. (a) Simulated S_{21} of the FSS in TE mode (θ pol). (b) Simulated S_{21} of the FSS in TE mode (Φ-pol).

In TE mode, maximum deviations of 0.83%, 1.67%, and 1.97% are found for low resonance frequencies ($\theta = 0°$ to 60°) using Equation (3), while maximum relative deviations of 0.40%, 0.80%, and 1.26% are obtained for high resonance frequencies. For resonance frequencies between ($\Phi = 0°$ and 60°), no deviations were observed; however, for higher resonance frequencies, extremely small relative deviations of 0.20%, 0.14%, and 0.16% were obtained. For TM mode, the minimal relative deviations are 0.41%, 0.38%, and 0.83% at low resonance frequencies and 0.40%, 0.96%, and 1.68% at high resonance frequencies ($\theta = 0°$ to 60°). No discrepancy was discovered for any polarization angle ($\Phi = 0°$ to 60°) for either low or high resonance values.

The proposed FSS is measured for its transmission coefficient to verify its polarization stability and angular stability. The FSS is tested in an anechoic chamber with the standard gain horn antennas. Measurements are carried out with pairs of X band horn antennas placed at the far field distance of 1 meter, and the FSS is rotated for the various incident angles. To verify the behaviour, the measurement was carried out by rotating the FSS with turn table and also rotating with the horn antenna. Measurements are taken for various incident angles, viz., 0, 30, and 60 degrees. From Figure 9, the measured results are in good agreement with the simulated results. The response at 60 degrees has additional ripples without much affecting the FSS behaviour. The measurement setup is depicted in Fig. 8. The measured results are compared with the simulated ones in Fig. 9.

Table 1 provides the comparison of proposed FSS with existing literature. We have considered single layer dual mode FSSs for appropriate comparison. From table, it is understood that the dual mode FSS is compact in this frequency range with reasonable bandwidth and exhibits stable response

Figure 8. Measurement setup for proposed antenna.

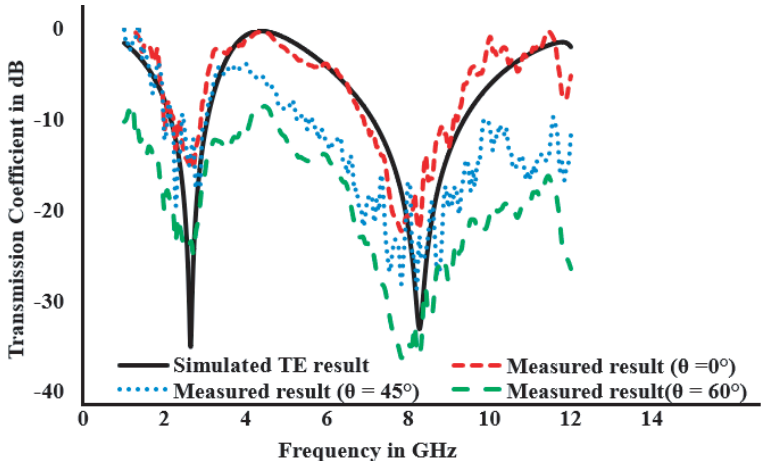

Figure 9. Comparison of measured transmission coefficient with simulated results.

Table 1. Comparison of proposed FSS with existing FSSs.

Ref.	Unit cell size	Layer/Band	Operating Frequency	Bandwidth	Application
[2]	$0.065\lambda_0 \times 0.076\lambda_0$	Single/Dual	2.4 GHz and 5 GHz	130 MHz	Dual WLAN frequency bands
[3]	$0.088\lambda_0 \times 0.088\lambda_0$	Single/Dual	2.54 to 3.54 GHz	315 MHz & 178.5 MHz	S-Band operation
[4]	$0.248\lambda_0$	Single/Dual	3.38 GHz and 7.3 GHz	1.05 GHz & 0.21 GHz	Wireless Application
[5]	$0.072\lambda_0$	Single/Dual	900 to 1790 MHz	91 MHz & 156 MHz	GSM shielding
[6]	$0.133\lambda_0$	Single/Dual	5.1–5.9 GHz & 3.7–4.3 GHz	0.5 GHz & 0.98 GHz	C & WLAN band application (satellite communication)
[8]	$0.078\lambda_0 \times 0.078\lambda_0$	Double/triple	GSM900, 1800, Wi-Fi2400 band	-	GSM, Wi-Fi
[12]	$0.106\lambda_0$	Triple/Triple	3.2 GHz–3.7 GHz, 4.1 GHz–6 GHz 8 GHz–12.1 GHz,	-	WiMAX, WLAN, X-band
[13]	$0.021\lambda_0$ & $0.035\lambda_0$	Triple/Dual	2.1 GHz (8.9 GHz–11 GHz), 3.5 GHz (30.1 GHz–33.6 GHz)	-	X and Ka band applications
[19]	$0.25\lambda_0$	Single/Single	10 GHz	-	Sub reflector for Wearable antenna & conformal shielding
[20]	$0.15\lambda_0$	Double/Dual	5.8 GHz & 7.6 GHz	5.10 GHz & 7 GHz (at −10 dB)	S, C and X band applications
Proposed Work	**$0.098\lambda_0$**	**Single/Dual**	**2–3 GHz & 8–10 GHz**	**0.2 GHz & 0.9 GHz**	**S (WLAN) & X-Band (RADAR & Military applications)**

up to 60° in both TE and TM modes. This can be implemented as a passive shield for S/X band applications.

4. CONCLUSION

This paper presents a dual band FSS design and its shielding performance at S band and X band. It provides dual stopband behaviour at S band with 200 MHz bandwidth and stopband at X band with 900 MHz bandwidth which finds its application in RADAR and military. The FSS behaviour is stable for TE mode and TM mode with the incident angles up to 60 degrees. The proposed dual mode FSS is of single layer which is compact compared with the existing work presented in literature. In future, there is a scope of improving the FSS bandwidth through double layer FSS.

REFERENCES

1. Yang, Y., X. H. Wang, and H. Zhou, "Dual-band frequency selective surface with miniaturized element in low frequencies," *Progress In Electromagnetics Research Letters*, Vol. 33, 167–175, 2012.
2. Yan, M., S. Qu, J. Wang, J. Zhang, H. Zhou, H. Chen, and L. Zheng, "A miniaturized dual-band FSS with stable resonance frequencies of 2.4 GHz/5 GHz for WLAN applications," *IEEE Antennas and Wireless Propagation Letters*, Vol. 13, 895–898, 2014.
3. Sivasamy, R. and M. Kanagasabai, "A novel dual-band angular independent FSS with closely spaced frequency response," *IEEE Microwave and Wireless Components Letters*, Vol. 25, No. 5, 298–300, 2015.
4. Neto, V. P. S., S. B. Paica, and A. G. D'Assunção, "A new compact dual-band FSS with angular and polarization stability for wireless applications," *2017 SBMO/IEEE MTT-S International Microwave and Optoelectronics Conference (IMOC)*, 1–4, IEEE, August 2017.
5. Yin, W., H. Zhang, T. Zhong, and X. Min, "A novel compact dual-band frequency selective surface for GSM shielding by utilizing a 2.5-dimensional structure," *IEEE Transactions on Electromagnetic Compatibility*, Vol. 60, No. 6, 2057–2060, 2018.
6. Jindal, P., A. Yadav, and S. K. Sharma, "Dual stop band frequency selective surface for C and WLAN band applications," *AEU — International Journal of Electronics and Communications*, Vol. 97, 267–272, 2018.
7. Zhang, J., L. Yan, R. X. K. Gao, C. Wang, and X. Zhao, "A novel 3D ultra-wide stopband frequency selective surface for 5G electromagnetic shielding," *2020 International Symposium on Electromagnetic Compatibility — EMC EUROPE*, 1–4, IEEE, September 2020.
8. Kumar, T. S. and K. J. Vinoy, "A miniaturized angularly stable FSS for shielding GSM 0.9, 1.8, and Wi-Fi 2.4 GHz bands," *IEEE Transactions on Electromagnetic Compatibility*, Vol. 63, No. 5, 1605–1608, 2021.
9. Zhang, K., X. Zhou, Z. Wei, and H. Zhai, "A low-profile dual-band antenna loaded with the AMC surface," *2017 Sixth Asia-Pacific Conference on Antennas and Propagation (APCAP)*, 1–3, IEEE, October 2017.
10. Ghosh, S. and K. V. Srivastava, "An angularly stable dual-band FSS with closely spaced resonances using miniaturized unit cell," *IEEE Microwave and Wireless Components Letters*, Vol. 27, No. 3, 218–220, 2017.
11. Nauman, M., R. Saleem, A. K. Rashid, and M. F. Shafique, "A miniaturized flexible frequency selective surface for X-band applications," *IEEE Transactions on Electromagnetic Compatibility*, Vol. 58, No. 2, 419–428, 2016.
12. Bashiri, M., C. Ghobadi, J. Nourinia, and M. Majidzadeh, "WiMAX, WLAN, and X-band filtering mechanism: Simple-structured triple-band frequency selective surface," *IEEE Antennas and Wireless Propagation Letters*, Vol. 16, 3245–3248, 2017.
13. Yan, M., S. Qu, J. Wang, A. Zhang, L. Zheng, Y. Pang, and H. Zhou, "A miniaturized dual-band FSS with second-order response and large band separation," *IEEE Antennas and Wireless Propagation Letters*, Vol. 14, 1602–1605, 2015.
14. Ünaldı, S., S. Cimen, G. Çakır, and U. E. Ayten, "A novel dual-band ultrathin FSS with closely settled frequency response," *IEEE Antennas and Wireless Propagation Letters*, Vol. 16, 1381–1384, 2016.

15. Sheng, X., J. Ge, K. Han, and X. C. Zhu, "Transmissive/Reflective frequency selective surface for satellite applications," *IEEE Antennas and Wireless Propagation Letters*, Vol. 17, No. 7, 1136–1140, 2018.
16. Khan, S. and T. F. Eibert, "A multifunctional metamaterial-based dual-band isotropic frequency-selective surface," *IEEE Transactions on Antennas and Propagation*, Vol. 66, No. 8, 4042–4051, 2018.
17. Ma, T., H. Zhou, Y. Yang, and B. Liu, "A FSS with stable performance under large incident angles," *Progress In Electromagnetics Research Letters*, Vol. 41, 159–166, 2013.
18. Yin, W., H. Zhang, T. Zhong, and Q. Chen, "A outstanding miniaturized frequency selective surface based on convoluted interwoven element," *Progress In Electromagnetics Research Letters*, Vol. 69, 133–139, 2017.
19. Yong, W. Y., S. K. A. Rahim, M. Himdi, F. C. Seman, D. L. Suong, M. R. Ramli, and H. A. Elmobarak, "Flexible convoluted ring shaped FSS for X-band screening application," *IEEE Access*, Vol. 6, 11657–11665, 2018.
20. Habib, S., G. I. Kiani, and M. F. U. Butt, "A convoluted frequency selective surface for wideband communication applications," *IEEE Access*, Vol. 7, 65075–65082, 2019.
21. Sharma, P., S. S. Kumar, M. B. Mahajan, and R. Jyoti, "Closely spaced tri resonance wide band FSS for S/Ku/Ka band," *2018 IEEE Indian Conference on Antennas and Propogation (InCAP)*, 1–5, IEEE, December 2018.
22. Katoch, K., N. Jaglan, S. D. Gupta, and M. S. Sharawi, "Design of a triple band notched polarization independent compact FSS at UWB frequency range," *International Journal of RF and Microwave Computer-Aided Engineering*, Vol. 31, No. 6, e22631, 2021.
23. Shafqat, M., M. M. Asim, F. Ahmed, and S. H. A. Bokhari, "An ultra-thin, flexible FSS with simultaneous stop-pass EM filtering," *2021 IEEE Region 10 Symposium (TENSYMP)*, 1–4, IEEE, August 2021.